Journal of Superconductivity and Novel Magnetism
https://doi.org/10.1007/s10948-023-06675-5

ORIGINAL PAPER

Two-Phase Microstructure Generated by Reaction of Nano WO_3 Addition and its Effect on Flux Pinning in Bi 2212 Composites

Pawan Kumar Verma[1] · B. Venkatesulu Reddy[1] · T. Rajasekharan[2] · Ramany Revathy[3] · Manoj Raama Varma[3] · V. Seshu Bai[1]

Received: 20 October 2023 / Accepted: 17 December 2023

Abstract
In the present work, Tungsten trioxide (WO_3) nanoparticles are added (up to 5 wt%) to $Bi_2Sr_{2.14}Ca_{0.86}Cu_2O_y$ (Bi 2212) compound using a sol-casting method that facilitates their uniform distribution in the Bi 2212 matrix. Sintering at 870 ºC, close to the melting point, has led to the formation of nearly spherical particles of WSr_2CaO_6 (W-alloy) phase (20–80 nm) by local reaction of distributed nano WO_3 particles with Bi 2212 grains. These particles are well dispersed and located preferentially at the platelet-like grain boundaries in the superconducting Bi 2212 composites. This is of interest in analogy to the widely studied $YBa_2Cu_3O_y$ (Y123) superconductor with two-phase microstructure with Y_2BaCuO_5 (Y211) precipitates, which is known to provide flux pinning and considerable enhancement of the critical current densities (J_c). The superconducting properties of the present Bi 2212 composites with varying amounts of second phase content are assessed by recording M-H loops at different temperatures 5 to 77 K. Critical current densities are found to be non-zero at 5 K in all the samples up to 9 T applied field, suggesting irreversibility fields to be above 9T. A considerable enhancement of J_c and flux pinning force are observed at temperatures 15–50 K, compared to pure 2212 phase at low concentrations (0.1 wt%) of nano WO_3 addition in the composites. A minor drop in the superconducting transition temperature T_c (onset) from 90 to 80 K observed in the sample with higher WO_3 addition (5 wt%) caused a lowering of flux pinning force at temperatures 50 K and above. Scaling laws of flux pinning show that normal surface pinning is the dominant mechanism in all the samples, which can be attributed to the structural defects at the 2212 platelet boundaries. Flux pinning is observed to be sustained in a broader field range and up to 50 K in all the samples with WO_3 addition. This provides evidence that the interfacial defects associated with the second phase (W-alloy) particles, created at the platelet boundaries, are effective in providing flux pinning.

Keywords Bi 2212 Superconductor · WO_3 Nanoparticles · Two-phase Microstructure · Flux Pinning · Scaling Behavior

1 Introduction

Bi 2212 is one of the important compounds of the $Bi_2Sr_2Ca_{n-1}Cu_nO_{2n+4+\delta}$ (BSCCO) family; Bi 2212 phase forms with a transition temperature (T_c) around 85 K at n = 2, and at n = 3, it is the Bi 2223 compound having T_c around 110 K [1]. Bi 2212 is the established high-temperature superconductor (HTSc), preferred for making superconducting wires/tapes having high critical density (J_c) for use at 4.2 K in high magnetic fields [2]. The common factors affecting the practical use of HTSc materials are high porosity, large anisotropy, and weak links between grains [3]. Repeated pressing and sintering at optimized temperatures are found to gain higher density [4] and show better performance in bulk or tapes.

✉ V. Seshu Bai
seshubai@uohyd.ac.in

[1] School of Physics, University of Hyderabad, Hyderabad 500046, India

[2] HYMOD advanced Products, TIDE-ASPIRE, University of Hyderabad, Hyderabad 500046, India

[3] National Institute for Interdisciplinary Science And Technology, Industrial Estate P.O. Pappanamcode, Thiruvananthapuram 695019, Kerala, India

The high transition temperature is an advantage for HTSc, when compared to conventional superconductors, but when it comes to practical applications, their performance deteriorates considerably even when a weak field is applied. The critical current density (J_c) decreases drastically due to the motion of flux lines and is referred to as flux creep [5, 6]. Introduction of defects of dimensions in the order of the coherence length (a few nm) of the superconductor works in providing pinning centres that pin the flux, thus improving superconducting properties, specially J_c.

Lattice defects like stacking faults [7, 8], dislocations [9], twin boundaries [10], etc., can pin the flux lines but are not easy to control as they depend on the processing conditions of superconductors. On the other hand, nanometer-sized pinning centres introduced by second-phase additions, if they can be controlled, can help in improving the physical properties of superconductors.

Many studies on introducing nano-sized secondary phases to BSCCO superconductors were reported that aim at improving the flux pinning properties. Various groups reported nano MgO addition to Bi 2212 bulk and superconductor tapes [11–13]. Wei et al. reported that, in comparison to the undoped sample, the addition of MgO enhanced flux pinning and effectively increased the irreversible field (B_{irr}) at 27 K [11].

Zhang et al. reported that Ag nanoparticle addition changed the thermodynamic properties of Bi 2212 superconductor; the intergrain coupling is strengthened, and J_c is improved. The addition of Ag nanoparticles with an average size of 5 nm were found to be embedded in the Bi 2212 matrix, improving J_c (to 4 kA/cm^2 till 6 T) at 4.2 K. The pinning mechanism operative was found to be surface pinning associated with the formation of highly crystalline grain boundaries caused by nano-Ag addition [14].

Nano ZrO_2 particle addition to Bi 2212 superconductor tape has led to the formation of (Ca,Sr)ZrO_3 precipitates of small size that are proposed to be effective pinning centres that caused improvement in flux pinning. However, J_c decreased with nano ZrO_2 addition at high fields, and the J_c for the undoped sample was better or comparable at all fields [15].

There are also reports of effective flux pinning by introducing nano ZrO_2 [16] and nano SiC [17] in the higher T_c phase Bi 2223. Adding 1 mass% nano MgO [18] into Bi 2223/Ag tapes was reported to enhance J_c. Excessive MgO (> 3 mass %) doping was found to damnify the transport properties due to agglomeration of MgO particles and increase of secondary phase fraction [18].

Berdan Ozkurt reported that adding nano WO_3 (40 nm) to $Bi_{1.8}Sr_2W_xCa_{1.1}Cu_{2.1}O_y$, x = 0, 0.05, 0.1, and 0.25 ceramics by solid-state synthesis route had adverse effects. T_c, J_c, and grain connectivity decreased with W content [19].

The addition of WO_3 to Bi 2223 by solid-state reaction [20] was found to react with the matrix phase, resulting in lowering of T_c and deterioration of superconducting properties, whereas recently Verma et al. reported that the addition of nano WO_3 to Bi 2223 in low concentrations (0.1 wt%) led to effective pinning and enhancement of J_c to higher fields [21].

We note from the above that the addition of secondary phases to the BSCCO superconductors does not always enhance the superconducting properties, especially at higher applied fields. Hence, the identification of suitable pinning centres and the methods to distribute them uniformly in the superconducting matrix without reaction is essential. A study of the role of different defects that are introduced by doping or those that form during processing, which can cause effective flux pinning at different field regimes, would be of immense importance. Such a study would help in designing superconducting composites with microstructures that would result in higher J_c, sustained to high applied fields.

In this direction, we have studied the effect of uniformly distributed nano WO_3, enabled by a sol-casting [22] process, into the Bi 2212 matrix. For the current study, we have added nano WO_3 particles in the size range of 2 to 12 nm to Bi 2212. Superconducting samples with different amounts of nano WO_3 addition were processed at temperatures close to melting point to facilitate a reaction and were characterized using various techniques. The current densities and flux pinning observed in samples with varying WO_3 content are analysed in the light of their microstructural details, as discussed below.

1.1 Experimental

In the present work, we synthesized composites of Bi 2212 with $Bi_2Sr_{2.14}Ca_{0.86}Cu_2O_y$ composition [23–26], chosen from a superconducting $Bi_2Sr_2(Ca_{0.86}Sr_{0.14})_{n-1}Cu_nO_y$ series by adding varying amounts of nano WO_3. The stoichiometric powders were prepared by nitrate route [27, 28]. For this, high-purity Bi_2O_3, $SrCO_3$, $CaCO_3$, and CuO were weighed out in stoichiometric ratios of the metal atoms, to synthesize the composition $Bi_2Sr_{2.14}Ca_{0.86}Cu_2O_y$, and were dissolved individually in concentrated Nitric acid and were mixed under continuous stirring. The solution was heated while stirring till it was converted to a blue color solid which was ground into a fine powder and calcined at 500 °C. The calcined powder was ground again and annealed thrice at 800 °C, with intermediate grinding to get precursor powder of Bi 2212.

WO_3 nanoparticles were synthesized by reacting Tungsten (W) metal powder with H_2O_2 [29]. Tungsten metal

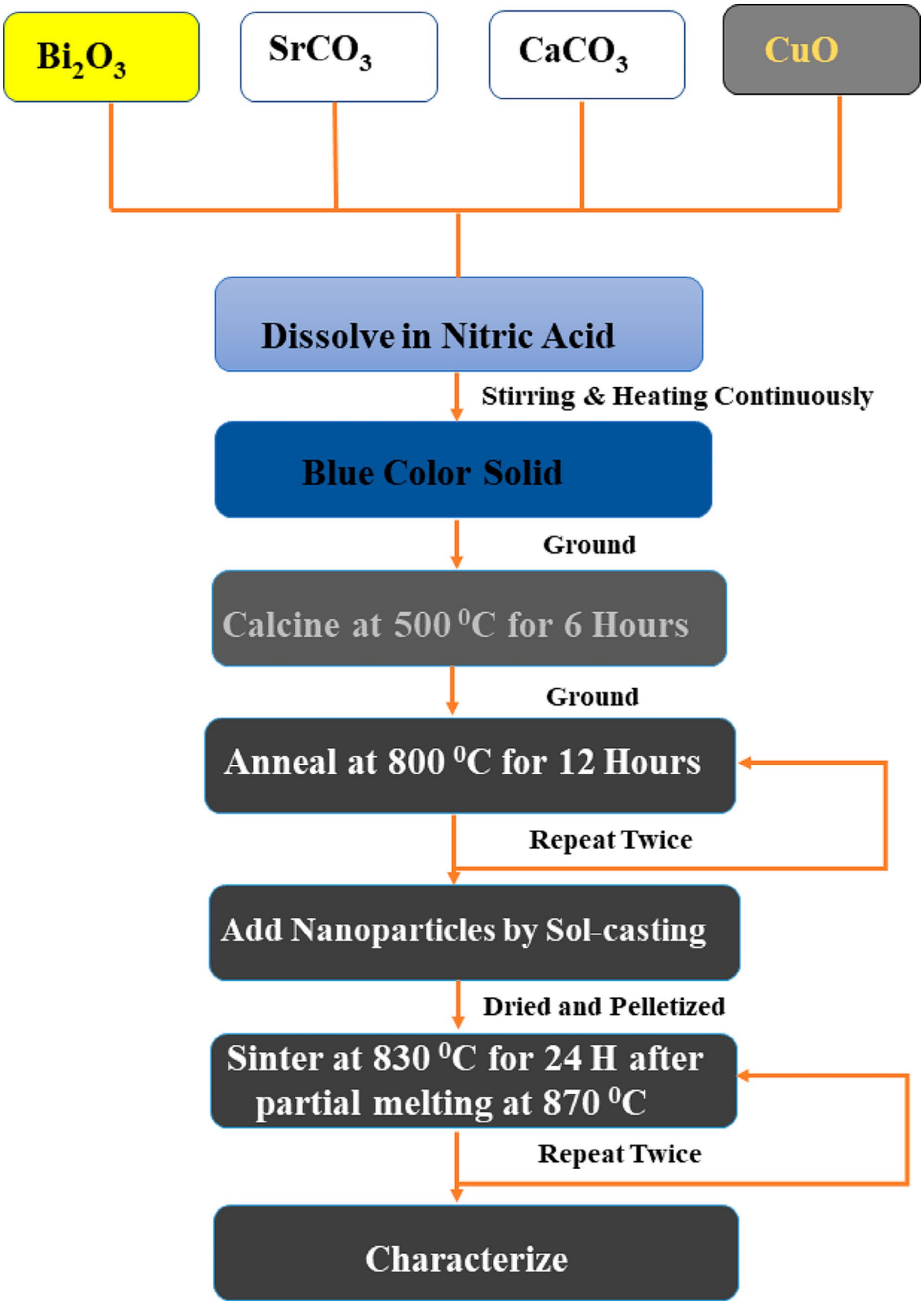

Fig. 1 Stepwise flow chart for sample preparation

powder was dispersed in a pre-cooled solution of distilled water and Hydrogen peroxide (MERCK, 30%). H_2O_2 reacts with W to give a solution of light-yellow color with suspended WO_3 nanoparticles. This solution was maintained for several hours at 273 K, using an ice bath to control the exothermic reaction. The solution was vacuum-dried to get WO_3 nanoparticles.

WO_3 nanoparticles thus obtained were added in different mass ratios to the fine powders of Bi 2212 by employing dispersive sol-casting method [22] that enables their uniform distribution in the matrix. In Sol-casting process a powder mix of Bi 2212 matrix phase and the WO_3 nanoparticles are suspended in a liquid medium consisting of a dispersant (Darvan 821), monomer (Methylacrylamlide), and cross-linker (N, N' methylenebisacrylamide) [19]. The resultant free-flowing slurry is tumbled for several hours and is polymerized by adding initiator (ammonium persulphate) and catalyst (Tetramethylethylenediamine) and then is dried. The dried powders were de-bindered by heating to 800ºC. This process prevents agglomeration of WO_3 nanoparticles in the Bi 2212 matrix.

Pellets of 20 mm diameter and nearly 5 mm thick were made using a uniaxial press at 12-Ton pressure. Pellets thus made were melted partially by heating at 870 °C for 30 min and then were sintered at 830 °C for 24 h to obtain Bi 2212 composites with nano WO_3 addition. The resultant samples were subjected to a second stage of pressing and sintering (referred to as press-sintering) for densification. A stepwise flow chart of sample preparation is given in Fig. 1. Bi 2212 composites thus synthesized with different amounts of nano WO_3 were coded as follows: Sample without WO_3 addition as WB 0, and with 0.1, 1, and 5 wt% nano WO_3 addition as WB 1, WB 2, and WB 3, respectively.

All the samples were characterized for phase formation by analyzing their X-ray diffraction patterns recorded (on Malvern Panalytical diffractometer) using Cu K_α radiation. Magnetic field (H) dependence of Magnetization (M) was recorded using PPMS (Quantum Design, Dynacool) at various Temperatures (T). The onset temperatures T_c (onset) of superconducting transitions were measured from M-T curves recorded for each sample, and the critical current density (J_c) was calculated at varying magnetic fields from the M-H loops recorded at various temperatures.

2 Results and Discussion

2.1 Characterization of WO_3 Nanoparticles

WO_3 nanoparticles were analyzed prior to adding to Bi 2212, using TEM and XRD. The TEM image in Fig. 2(a & b) of WO_3 nanoparticles shows that the particles were in the 2–12 nm size range. Analysis of XRD pattern confirms the formation of WO_3 with an orthorhombic structure. The lattice parameters are a = 7.320(9) Å, b = 7.704(9) Å, and c = 7.535(6) Å. The indexed XRD pattern of WO_3 particles is shown in Fig. 2(c).

2.2 XRD Analysis of Bi 2212 Composites

Indexed X-Ray Diffraction (XRD) patterns for all the Bi 2212 composite samples are given in Fig. 3. Majority of the peaks in the XRD patterns could be indexed to Bi 2212 as the main phase. X'pert Highscore Plus software was used for phase identification and lattice parameter analysis.

Small amounts of the low T_c phase $Bi_2Sr_2CuO_6$ (Bi 2201) and traces of other oxide phases, are seen as indicated in Fig. 3.

For sample WB 2 having 1 wt% or more of nano WO_3 addition, the formation of a second phase was detected, which could be indexed to WSr_2CaO_6 compound. The diffraction peaks observed at 2 theta values 18.83, 36.48, 44.2, and 55.04 represent the presence of this phase. Using Highscore software it was estimated that the amount of WSr_2CaO_6 phase increased from 6.6% for sample WB 2 to ~20% in sample WB 3 with 5 wt% of WO_3 addition.

The amount of the WSr_2CaO_6 phase has increased with the rise in WO_3 content, confirming that nano WO_3 reacted with matrix phase elements during the heating process to form this phase. A slight shift in the lattice parameters was also observed with nano WO_3 addition, compared to sample WB 0, which suggests that a small amount of W enters the unit cell, probably substituting for Cu, due to their comparable ionic radii [30]. Lattice parameters and the phases present in all the samples are given in Table 1.

2.3 Microstructural Analysis

Figure 4 shows the FESEM images of microstructures of fractured surfaces in all the samples. All samples have closely packed platelet-like grains. In samples with addition of nano WO_3 (mostly of size 2–6 nm), spherical particles (20–80 nm size) of a second phase have formed and are found located systematically at the platelet boundaries.

Number of the spherical particles was observed to increase with increasing WO_3 addition. Energy dispersive X-ray (EDAX) analysis in the region of the particles in WB 2 and WB 3 showed a composition containing W-Sr-Ca-O phase. It was difficult to assess the exact composition of the particles due to their small size. Combining the results from XRD analysis, we identify the particles to be of WSr_2CaO_6 phase. It is interesting to note that the nano WO_3 particles have reacted locally with the elements of the matrix phase and formed a two-phase microstructure akin to

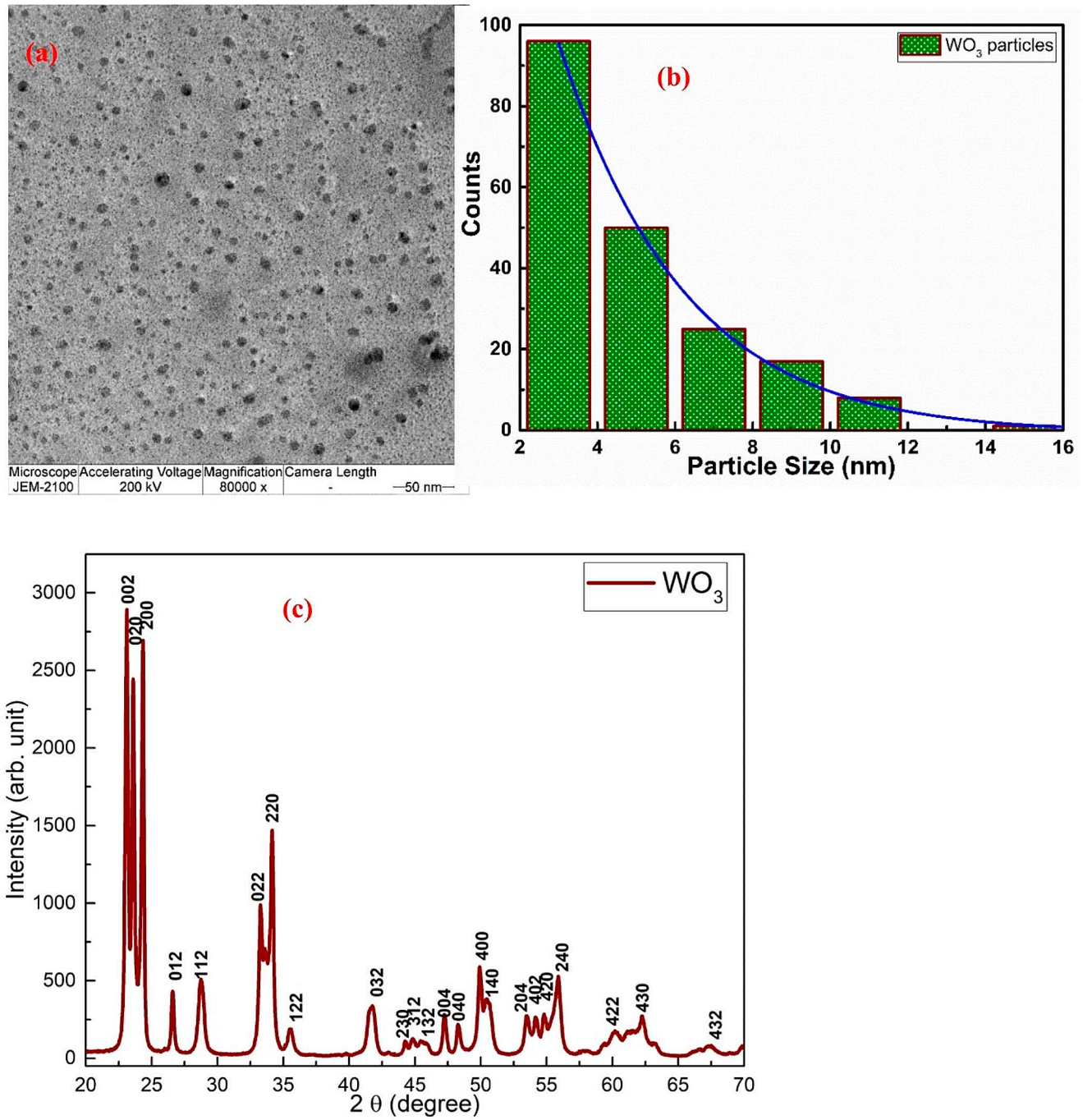

Fig. 2 (**a**) TEM image showing WO_3 nanoparticles dispersed in liquid medium, (**b**) Histogram shows that most particles are in the 2–6 nm range, (**c**) Indexed XRD pattern for WO_3 nanoparticles

Y 123 with Y 211 precipitates [10, 31–34]. We believe that uniform distribution of second phase WSr_2CaO_6 particles in Bi 2212 observed in Fig. 4, is a result of the local reaction of uniformly distributed nano WO_3 in the matrix without agglomeration, which was possible through the sol-casting method used in this work. The fact that the number density of these precipitates can be controlled by varying the nano WO_3 content is significant in optimizing microstructures for improved properties.

2.4 Temperature Dependence of Magnetization

Figure 5 shows the temperature dependence of magnetization (M) recorded for all Bi 2212 samples with nano WO_3 addition, in the temperature range 20–120 K under 5 mT

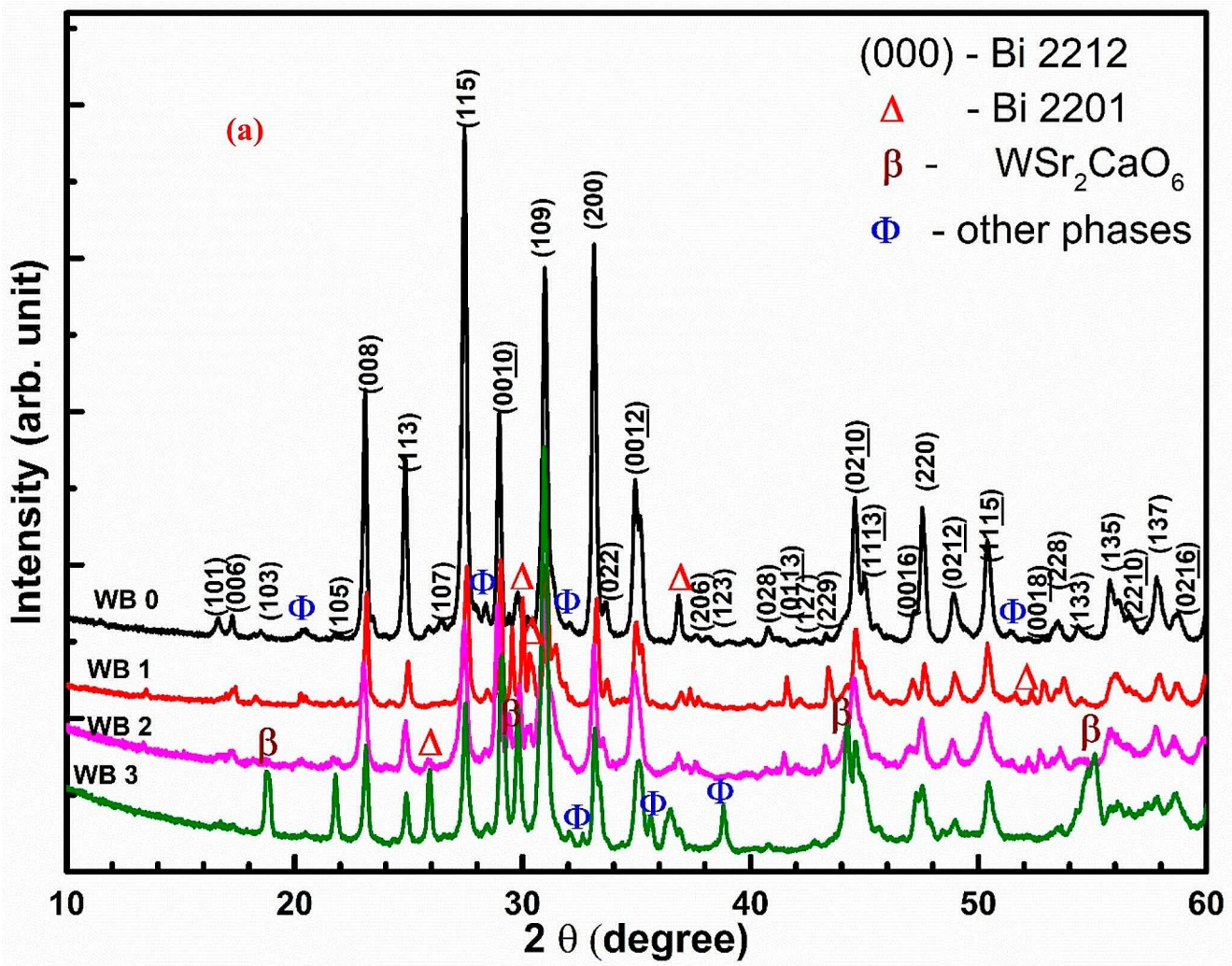

Fig. 3 : Indexed XRD patterns for all the Bi 2212 samples with nano WO_3 addition showing Bi 2212 as the main phase present. Minor amounts of Bi 2201 (marked Δ) and other oxide phases (marked **Φ**) are seen. At higher concentrations of WO_3, the formation of WSr_2CaO_6 (marked **β**) phase was observed

Table 1 Lattice parameters and phase identification for all Bi 2212 samples with nano WO_3 addition

Sample	Lattice parameters of 2212 phase			Traces of Minority phases present	Other impurity phases
	a (Å)	b (Å)	c (Å)		
WB 0	5.405(6)	5.407(7)	30.817(7)	Bi 2201 (**Δ**), Bi-Sr-O and Sr-Cu-O (**Φ**)	
WB 1	5.411(6)	5.418(4)	30.905(1)	Bi 2201 (**Δ**), Bi-Sr-O (**Φ**)	
WB 2	5.414(7)	5.415(8)	30.916(6)	Bi 2201 (**Δ**), Bi-Sr-O (**Φ**)	WSr_2CaO_6 (**β**) 6.6%
WB 3	5.414(5)	5.414(2)	30.855(5)	Bi 2201 (**Δ**)	WSr_2CaO_6 (**β**) 20.8%

applied field. The occurrence of diamagnetic transition in the range 80–90 K confirms the formation of Bi 2212 as the majority phase in all the samples. For the sample WB 0, with no nano WO_3 addition, T_c (Onset) is around 90 K while 5 wt% nano WO_3 added sample exhibits the lowest T_c (Onset) of around 80.5 K. We observe that the T_c (onset) reduced from 90 to 80 K with nano WO_3 addition and that the superconducting fraction decreased gradually. This supports the possible substitution of W in the unit cells of Bi 2212, possibly at Cu site, as discussed in XRD analysis. Change of T_c owing to the substitution of certain ions of comparable radii into the lattice is widely reported [35–39]. In the present system, the decrease in T_c is marginal and hence would affect the properties only close to T_c.

The transition widths (ΔT_c) were calculated, using the definition $\Delta T_c = T_c^{90\%} - T_c^{10\%}$ [40], from the normalized M-T

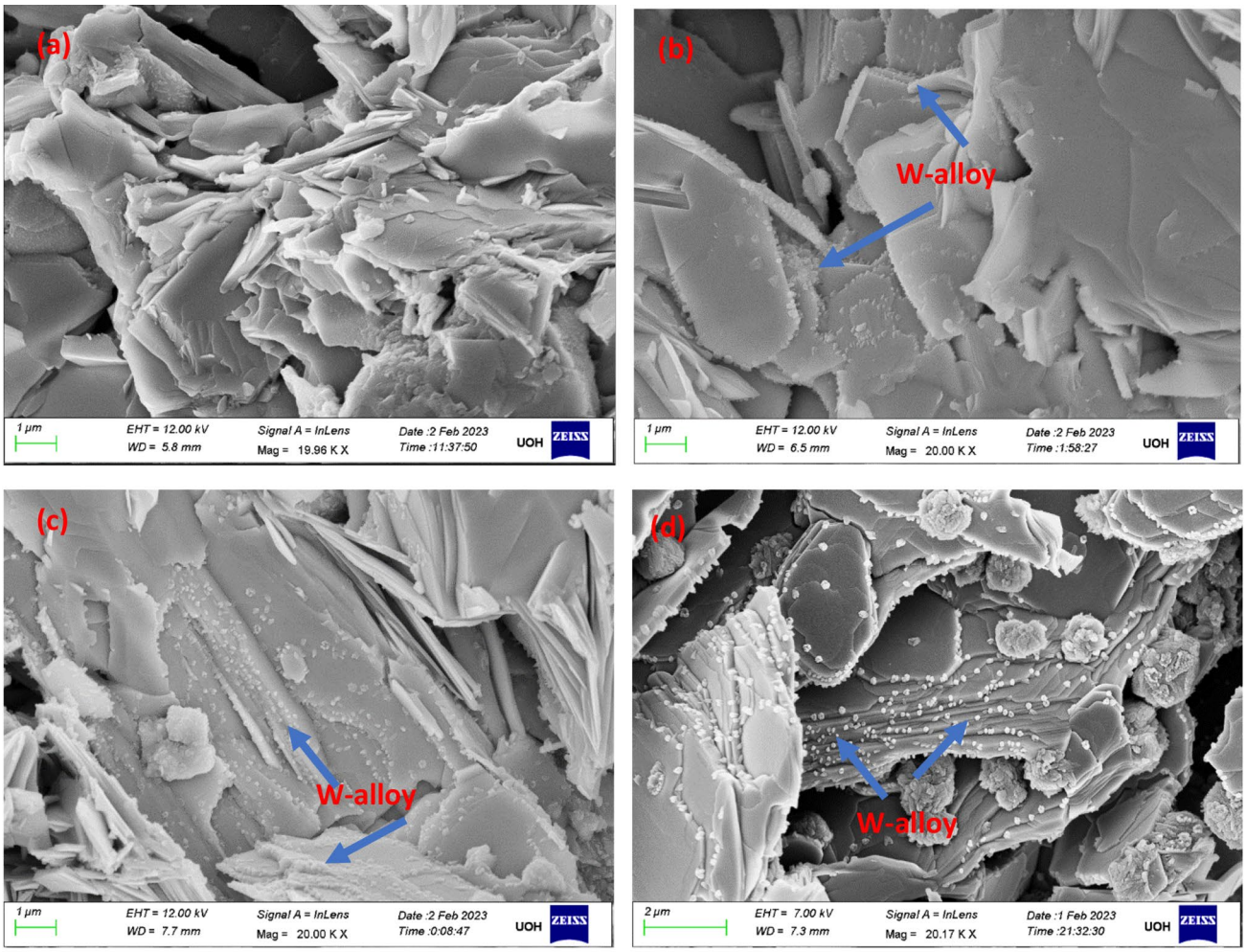

Fig. 4 (a-d): FESEM micrographs of fractured surfaces of all Bi 2212 samples with nano WO_3 addition; W w-containing phase observed are marked for samples WB 1, WB 2, and WB 3

curves shown in Fig. 5 and are given in Table 2. Here, $T_c^{10\%}$ and $T_c^{90\%}$ are the temperatures at which the diamagnetic signal strength falls to 10% and 90%, respectively, of the total drop across the transition. Samples WB 1 and WB 2 have relatively lower transition widths, ΔT_c. Transition widths of the order of 20 to 40 K are reported in Bi 2212 superconductors, for instance with Yb substitutions [41] and Au addition [42].

2.5 Field Dependence of Magnetization

Magnetic hysteresis (M-H) loops are recorded in all the samples at temperatures 5, 15, 50, and 77 K. Typical set of loops recorded at 5 K for all the samples is shown in Fig. 6. The hysteresis in M (opening of an M-H loop) is proportional to critical current density (J_c). At 5 K, M-H loops for all the samples are open till 9 T, indicating that all the samples have $J_c > 0$ up to the highest applied fields and hence have an irreversibility field B_{irr} of above 9 T.

The Critical current density for all the samples was calculated using Bean's critical state model [43], from the relation

$$J_c = 20\Delta M/d \tag{1}$$

ΔM is the hysteresis in magnetization, in emu/cc, measured from the curves recorded with increasing and decreasing fields.

Here, $d = a(1 - a/3b)$, a and b (a< b) are dimensions of the cross-section of the sample.

The field dependence of J_c for all the samples is shown in Fig. 7 (a & b) at 5 and 15 K. At 5 K, samples WB 0 and WB 1 have nearly equal J_c at lower fields, but at higher fields, the J_c for sample WB 0 decreases rapidly compared to that of WB 1. At 15 K, the sample WB 1 exhibits substantial enhancement in J_c and has the highest value among all the samples in the entire field range.

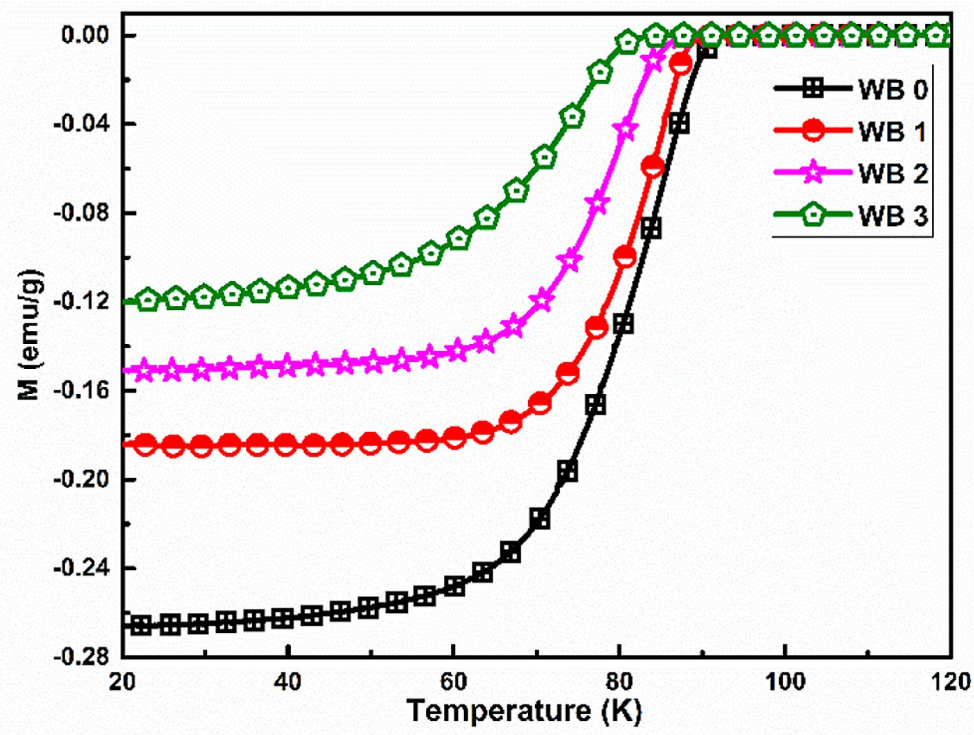

Fig. 5 Temperature dependence of magnetization for all Bi 2212 samples with nano WO_3 addition, showing an increased shift in the onset of diamagnetic transition to low temperatures with an increase in WO_3 content

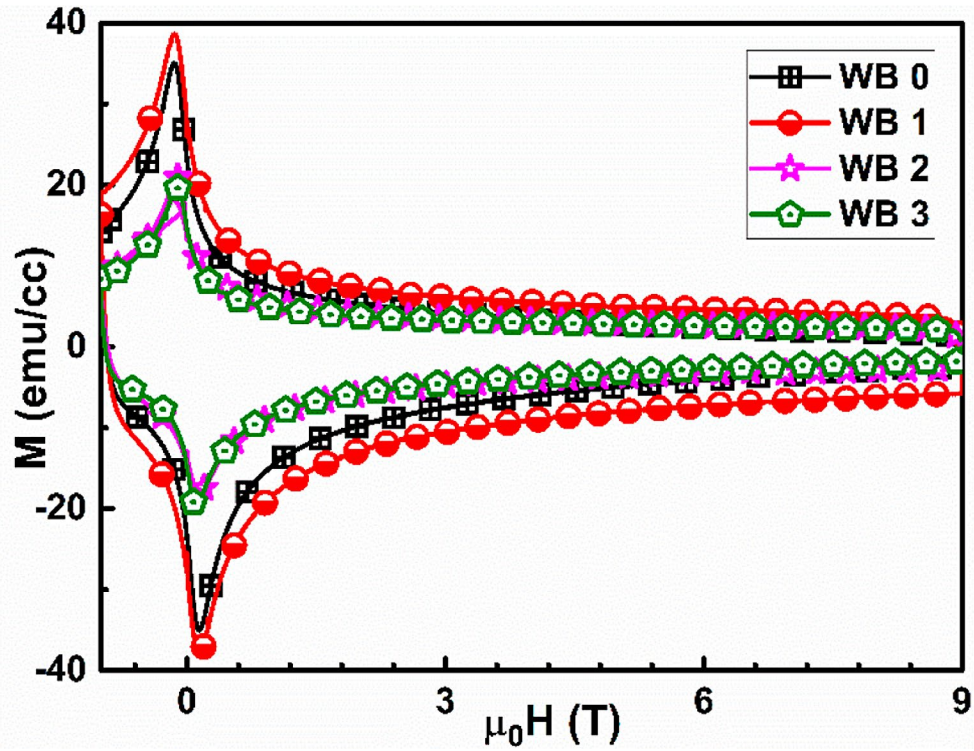

Fig. 6 Field dependence of magnetization for Bi 2212 samples with nano WO_3 addition at 5 K, showing all the samples have $J_c > 0$, till 9 T applied field

Table 2 Transition temperatures and transition widths for Bi 2212 samples with nano WO_3 addition

S. No.	Sample	T_c (K)	ΔT_c (K)
1	**WB 0**	90	23.2
2	**WB 1**	88.2	16.5
3	**WB 2**	85	18.2
4	**WB 3**	80.5	29.2

It can also be seen from Fig. 7 (c) that the fall in J_c with T is much more rapid in WB 0 with no nano WO_3 addition. J_c for sample WB1, with 0.1 wt% WO_3 is higher than for WB 0, in the temperature range 10 to 50 K. For WB 1 sample $J_c(0)$ value has increased by 60% at 15 K and by 35% at 50 K, with respect to those of WB 0. This suggests that the pinning centres generated by low concentrations of nano WO_3 addition are effective in the intermediate temperature range. All samples retained superconductivity up to 77 K.

Here, we bring in an analogy to the $YBa_2Cu_3O_{7-\delta}$ superconductor (called YBCO or Y 123) system in which distribution of 30 mol % of non-superconducting Y 211 particles in Y 123 matrix leads to substantial enhancement of J_c [44, 45]. This is attributed to flux pinning caused by fine secondary defects like stacking faults generated at the interface of the particles with the matrix phase. The secondary defects are of size comparable to the coherence length of HTSCs, as observed from spectroscopic investigations [10, 33, 46].

From this, we infer optimum levels of defect density generated by the W- alloy phase (WSr_2CaO_6) particles present in the Bi 2212 matrix in WB 1 sample, which appears to have provided effective flux pinning retaining higher J_c as observed in Fig. 7(b) to higher fields. The $J_c(0)$ values, (i.e. J_c at zero field) are given in Table 3 for all the samples at different temperatures.

2.6 Analysis of Flux Pinning Force Density (F_p)

For an in-depth understanding on pinning of flux occurring in Bi 2212 composite samples, the flux pinning force density (F_p) is calculated using the relation, $F_p = J_c x\ B$ and is analysed in terms of scaling laws.

The field dependences of flux pinning force density at 5, 15, and 50 K are shown in Fig. 8 (a-c). At 5 K, F_p monotonically increases with field for all the samples with WO_3 addition, while it reaches a maximum at about 5 T for

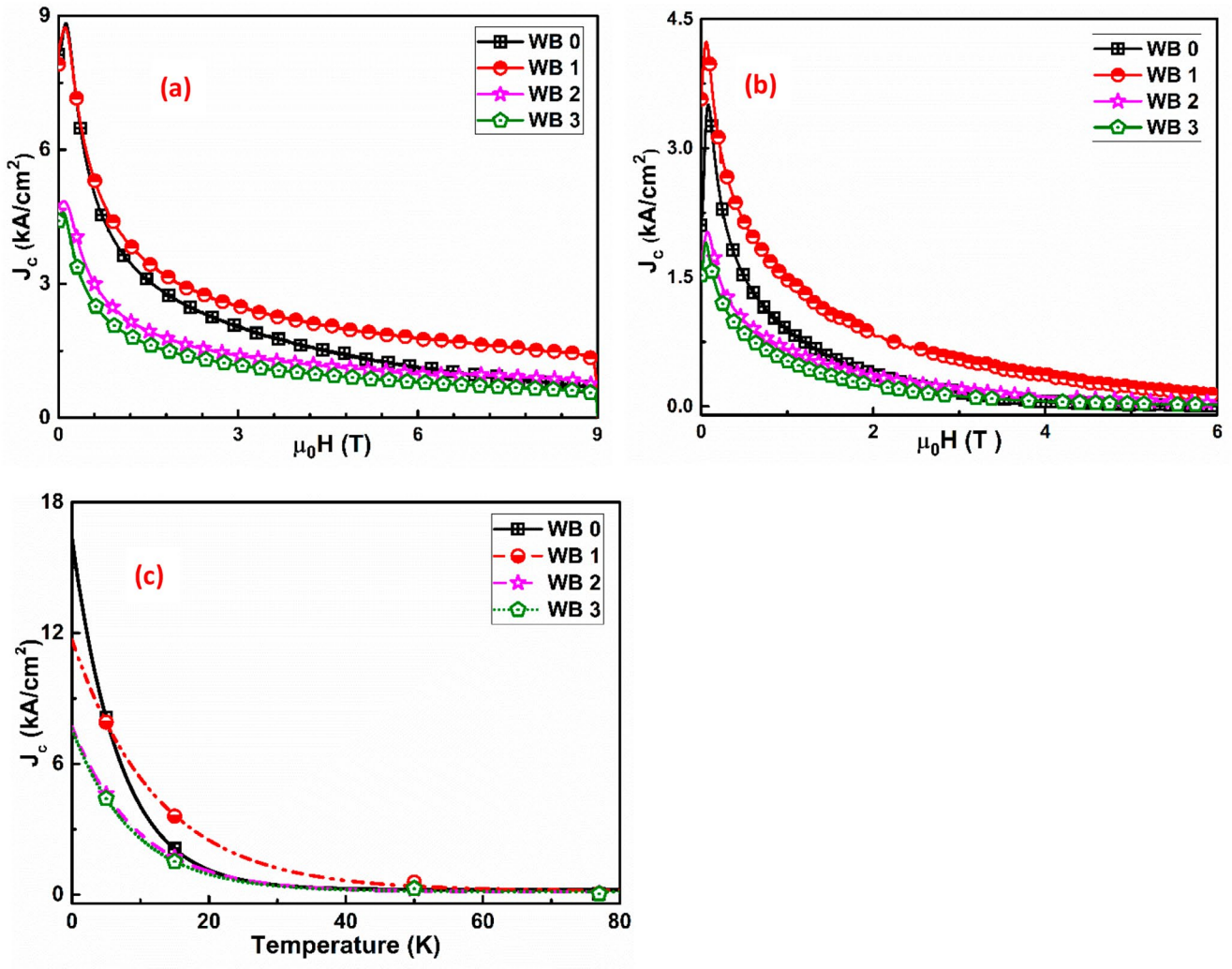

Fig. 7 Field dependence of J_c at (a) 5 K and (b) 15 K respectively; (c) T dependence of zero field J_c in the range 5 to 77 K, for all the samples of Bi 2212 series with nano WO_3 addition

WB 0. This shows that flux lines remain pinned till the 9 T applied field in the composites, suggesting suppression of flux creep, compared to WB 0, even at low temperatures. The F_p has the highest value for WB 1 when compared to other samples at all temperatures. The $F_{p\ max}$ values for all the samples are given in Table 3.

At higher temperatures like 15 and 50 K, the $F_{p\ max}$ (the peak value of F_p in the F_p vs. B ($B = \mu_o H$) curves) shifts to lower fields for all the samples, due to flux creep that is known to be predominant in BSCCO superconductors compared to YBCO [47, 48] superconductors and it increases with rise in temperature. However, for WB 1 sample, $F_{p\ max}$ occurs at higher fields at all temperatures, compared to all other samples. This suggests that at low concentrations of WO_3, effective flux pinning is achieved to higher fields. The full width at half maximum (FWHM) of F_p vs. B curves is a measure of the range of fields in which pinning is effective and is found to be 5.45 T at 15 K for WB 1, while it is 2.9 T for WB 0, as can be seen from Fig. 8(b). The fact that the peak widths of F_p vs. B curves for WB 1 sample are larger till 50 K confirms the effective field range of flux pinning to have been enhanced by the defects generated by adding 0.1 wt% nano WO_3 to Bi 2212.

Studies on the pinning mechanism in BSCCO samples in literature, propose normal surface pinning at grain boundaries (δl pinning) to be dominant [49, 50] while substitutional defects and the presence of low T_c superconducting phases, if any, would cause δT_c pinning [51]. In the present set of composites, we find that pinning from the defects generated by the reaction of nano WO_3 is also effective, in addition to the structural defects at platelet/grain boundaries, leading to additional surface pinning in composites over a broader field range compared to that of WB 0, as seen in Fig. 8 (a-c). Small amounts of Bi 2201 phase (with a T_c of 10 K) present become normal and contribute marginally to flux pinning at all temperatures above 10 K.

To understand the nature of pinning present in our samples, we plotted the normalized pinning force ($f = F_p/F_{p\ max}$) vs. h ($= B/B_p$) along with the theoretical curve for Normal surface pinning mechanism as discussed in the literature [14, 52–54]. For this, field is normalized to peak field B_p (i.e. field at $F_{p\ max}$) such that $h = B/B_p = \mu_0 H/\mu_0 H_p$.

The scaling laws in terms of h [14, 49, 50, 52–55] for normal point pins and surface pinning are given by Eqns. below and are indicated by the continuous curves in Fig. 8(d & e).

For normal point Pinning.

$$f(h) = \frac{9}{4}h\left(1 - \frac{h}{3}\right)^2 \tag{2}$$

For normal surface Pinning.

$$f(h) = \frac{25}{16}h^{1/2}\left(1 - \frac{h}{5}\right)^2 \tag{3}$$

It can be seen from Fig. 8 (d &e), that the experimental curves are closer to the theoretical curve for normal surface pinning at 15 and 50 K. The deviation from theoretical curve at fields well above B_p is attributed to additional pinning mechanisms that operative at higher fields. At 5 K, the maximum in F_p is not reached even up to 9 T for the composites; hence, further analysis in terms of scaling laws was not considered at this temperature.

From Kramer's approach, we determined B^*, the characteristic field beyond which the rigidity of the flux line lattice (FLL) effectively vanishes, and B^* is $< B_{c2}$ in HTSc due to flux creep. B^* was obtained by linear extrapolation to zero of the low- J_c segment of the Kramer curve [56] in which $J_c^{1/2}B^{1/4}$ is plotted vs. field B. This approach of obtaining B^* is reported by [14, 57, 58]. Figure 8(f) shows a typical plot for sample WB 3 from which B^* is determined. B^* values at 15 and 50 K are shown in Table 3.

Lower transition widths indicative of better grain connectivity would also play a role in the superior superconducting properties observed for samples WB 1 and WB 2. Since Sample WB 0 has no nano WO_3 addition, there is an inadequacy of pinning centres to provide effective pinning at higher fields and this explains the rapid fall in J_c in WB 0 at higher fields.

According to reports based on computer simulations of the interactions between pinning centres and flux lines, at high defect densities, the mobility of the flux lines increases such that the flux lines can jump freely from one defect to another without being pinned [59, 60]. This might be the cause as to why the presence of secondary phases is effective only at low concentrations, and the superconducting properties start to degrade at higher concentrations.

Table 3 B^* (T) at 15 and 50 K, $J_c(0)$ *and* $F_{p\ max}$ at 5, 15, and 50 K for the Bi 2212 samples with varying nano WO_3 addition

Sample	15 K	50 K	5 K		15 K		50 K	
	B^* (T)	B^* (T)	$J_c(0)$ A/cm^2	$F_{p\ max}$ N/cm^3	$J_c(0)$ A/cm^2	$F_{p\ max}$ N/cm^3	$J_c(0)$ A/cm^2	$F_{p\ max}$ N/cm^3
WB 0	6.37	0.20	8124.5	870.7	2109.2	113.9	421	1.22
WB 1	8.35	0.32	7908.1	1566.4	3602.5	218.1	570.5	2.1
WB 2	8.55	0.24	4617.7	914.8	1697.3	90.8	260.8	0.77
WB 3	7.0	0.14	4408.1	662.8	1524	68.4	282.8	0.35

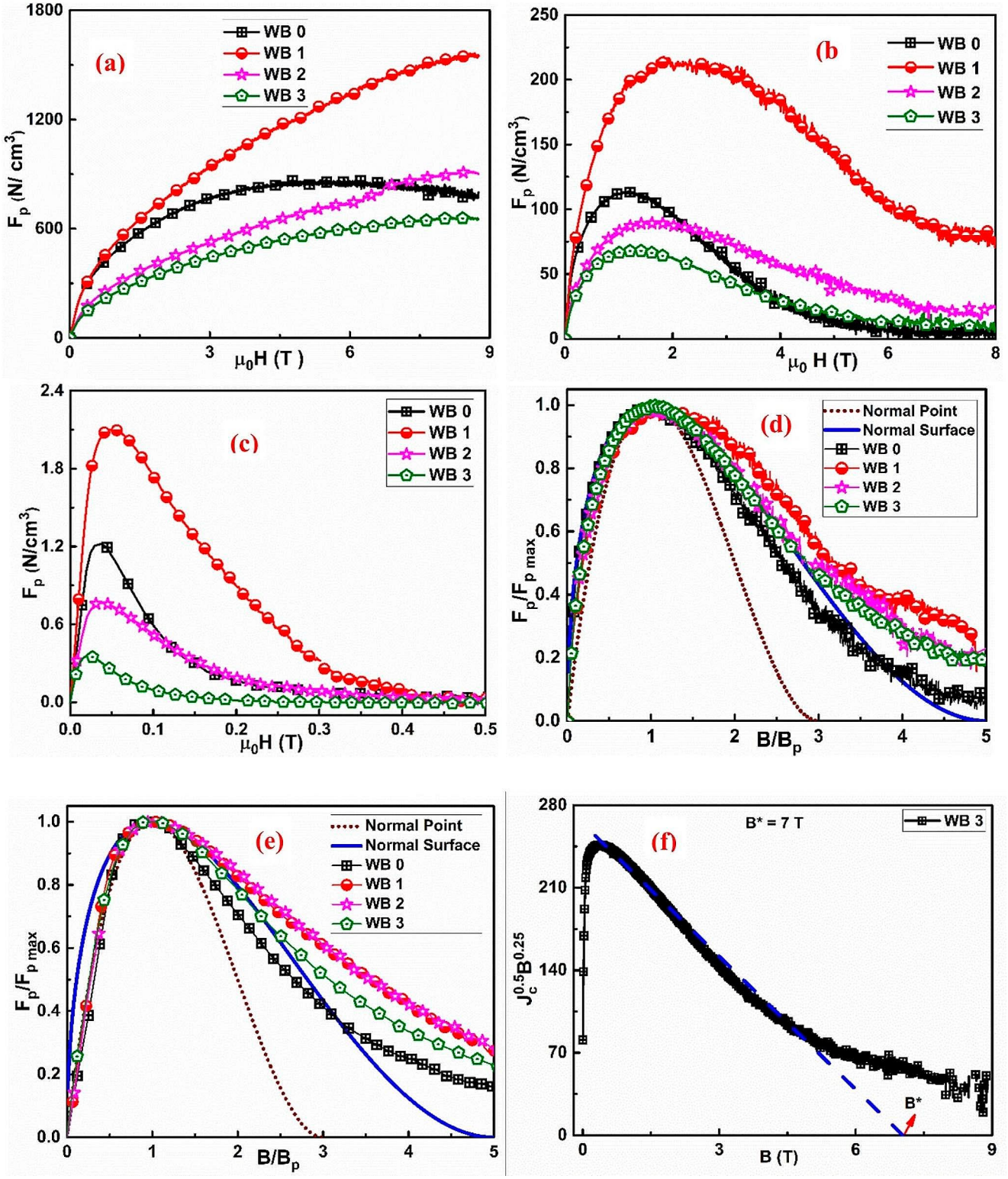

Fig. 8 **(a-c)**: Field dependence of Pinning force density at 5, 15, and 50 K respectively, (**d**, **e**) *f* vs. B/B_p curves along with theoretical curve (Eq. (2)) at 15 and 50 K respectively for all the Bi 2212 samples with nano WO_3 addition, (**f**) B^* estimation, shown typically, for sample WB 3 at 15 K, using Kramer's approach

Flux pinning from various sources/ mechanisms can thus simultaneously exist to different extents in high T_c superconductors and can be effective at different field and temperature regimes. However, separating the contributions from each of these sources to flux pinning quantitatively is a complex problem.

3 Conclusions

With an aim to mimic the two-phase microstructure of YBCO system that leads to effective flux pinning and enhanced J_c, we have investigated the effect of nano WO_3 addition on the superconducting properties of $Bi_2Sr_{2.14}Ca_{0.86}Cu_2O_y$ superconductor. Nano WO_3 particles that are uniformly distributed by sol-casting method into Bi 2212 matrix, which, on heating to 870ºC for a short duration, have generated nearly spherical particles (20–80 nm) of WSr_2CaO_6 as a second phase. These particles are seen to be well dispersed along the Bi 2212 platelet boundaries, as observed in FESEM images of fractured samples.

The number of second-phase particles generated increased with the amount of nano WO_3 added, confirming their formation due to the local reaction of nano WO_3 with the matrix phase. M-H loops recorded show B_{irr} to be above 9 T at 5 K in the composites, which is higher compared to pure Bi 2212 sample having B_{irr} around 5 T. Addition of nano WO_3 in low concentrations (0.1 wt%) is found to enhance the superconducting properties of Bi 2212 in a broad range of fields at intermediate temperatures of 10 to 50 K. The reason for the superior properties in composite is attributed to the effective flux pinning caused by the secondary defects created at the interface of the WSr_2CaO_6 particles with the matrix. Lowering of zero-field J_c at higher concentrations of nano WO_3 addition to Bi 2212 superconductors has a correlation to the reduction in the superconducting fraction. Detailed analysis of pinning force density using scaling laws suggests that more than one pinning mechanism can be operative at different field and temperature regimes. Our results show that flux pinning in a broad range of fields could be sustained to high fields by controlling the two-phase microstructure.

The current study reveals that the sol-casting method outperforms the conventional solid-state synthesis method for introducing suitable nanoparticles uniformly, without agglomeration, in Bi 2212 matrix. When the WO_3 nanoparticles are added by solid-state synthesis method, the J_c value diminished to zero around 5 T applied field at 4.2 K [19] whereas, for WO_3 nanoparticles added by sol-casting method, as in sample WB 1, the J_c falls nearly 4 times the $J_c(0)$ value but is sustained to 2 kA/cm^2 at 5 K till 9 T applied field. The reports in the literature suggest that the addition of nano-sized silver to Bi 2212 led to the fall of J_c approximately 100 times the $J_c(0)$ value, even at 4.2 K at 6 T applied field [14]. Nanosized Al precipitates added to Bi 2212 similarly resulted in rapid deterioration of J_c by 5 T field at 4.2 K [61]. At 10 K, in nano SiO_2 added Bi 2212 samples, the J_c diminished by around 3 T applied field [62]. Hence, in comparison to existing literature, nano WO_3 particles are a better choice as pinning centres to pin the flux lines at relatively higher fields, compared to peak field in $F_p(B)$ curves, and in 10 to 50 K temperature range.

The fact that the present Bi 2212 composites exhibit a two-phase microstructure, as in the YBCO system, with controllable second phase particle density opens up scope to design suitable microstructures in BSCCO superconductors with local reaction of suitable nanoparticles for improved flux pinning.

Acknowledgements VSB acknowledges DST- SERB for funding of a project, EMR 2016/006004. PKV is grateful to DST for fellowship. The authors are grateful to Mr. U. Govind and Dr. M. Sai Rama Krishna, IITH, Hyderabad for the TEM images of WO_3 nanoparticles. Useful discussions with Dr. U. Syamaprasad, NIIST and Prof. S. Srinath, UoH are gratefully acknowledged.

Declarations

Competing interests The authors declare that they have no known competing financial interests or personal relationships that could have appeared to influence the work reported in this paper.

References

1. Maeda, H., Tanaka, Y., Fukutomi, M., Asano, T., Togano, K., Kumakura, H., Uehara, M., Ikeda, S., Ogawa, K., Horiuchi, S., Matsui, Y.: New high-T_c superconductors without rare earth element. Phys. C Supercond its Appl. **153–155**, 602–607 (1988). https://doi.org/10.1016/0921-4534(88)90727-7
2. Kametani, F., Jiang, J., Matras, M., Abraimov, D., Hellstrom, E.E., Larbalestier, D.C.: Comparison of growth texture in round Bi2212 and flat Bi2223 wires and its relation to high critical current density development. Sci. Rep. **5**, 1–9 (2015). https://doi.org/10.1038/srep08285
3. Bulaevskii, L.N., Daemen, L.L., Maley, M.P., Coulter, J.Y.: Limits to the critical current in high- T_c superconducting tapes. Phys. Rev. B. **48**, 13798–13816 (1993). https://doi.org/10.1103/PhysRevB.48.13798
4. Kumar, R.R., Aloysius, R.P., Bose, R.J., Guruswamy, P., Syamaprasad, U.: Preparation of dense, high J_C Bi-2223 superconductors by multistage cold pressing. Supercond Sci. Technol. **18**, 689–693 (2005). https://doi.org/10.1088/0953-2048/18/5/018
5. Chikumoto, N., Konczykowski, M., Motohira, N., Malozemoff, A.P.: Flux-creep crossover and relaxation over surface barriers in $Bi_2Sr_2CaCu_2O_8$ crystals. Phys. Rev. Lett. **69**, 1260–1263 (1992). https://doi.org/10.1103/PhysRevLett.69.1260
6. Lykov, A.N.: Magnetic flux creep in HTSC and Anderson-Kim theory (review article). Low Temp. Phys. **40**, 773–795 (2014). https://doi.org/10.1063/1.4896968
7. Yamada, Y., Takahashi, K., Kobayashi, H., Konishi, M., Watanabe, T., Ibi, A., Muroga, T., Miyata, S., Kato, T., Hirayama, T.,

Shiohara, Y.: Epitaxial nanostructure and defects effective for pinning in Y(RE)$Ba_2Cu_3O_{7-x}$ coated conductors. Appl. Phys. Lett. **87**, 1–3 (2005). https://doi.org/10.1063/1.2061874
8. Eley, S., Glatz, A., Willa, R.: Challenges and transformative opportunities in superconductor vortex physics. J. Appl. Phys. **130** (2021). https://doi.org/10.1063/5.0055611
9. Shi, D., Chen, J.G., Welp, U., Boley, M.S., Zangvil, A.: Lattice defects and flux pinning in crystallized metal-oxide glasses in the bi-sr-ca-cu-o system. Appl. Phys. Lett. **55**, 1354–1356 (1989). https://doi.org/10.1063/1.101896
10. Devendra Kumar, N., Rajasekharan, T., Gundakaram, R.C., Seshubai, V.: Extensive nanotwinning: Origin of high current density to high fields in preform-optimized infiltration-growth-processed $YBa2Cu_3O_{7-\delta}$ superconductor. IEEE Trans. Appl. Supercond. **21**, 3612–3620 (2011). https://doi.org/10.1109/TASC.2011.2168819
11. Wei, W., Schwartz, J., Goretta, K., Balachandran, U., Bhargava, A.: Effects of nanosize MgO additions to bulk $Bi_{2.1}Sr_{1.7}CaCu_2O_x$. Phys. C Supercond. **298**, 279–288 (1998). https://doi.org/10.1016/S0921-4534(97)01889-3
12. Christova, K., Manov, A., Nyhus, J., Thisted, U., Herstad, O., Foss, S., Haugen, K., Fossheim, K.: $Bi_2Sr_2CaCu_2O_x$ bulk superconductor with MgO particles embedded. J. Alloys Compd. **340**, 1–5 (2002). https://doi.org/10.1016/S0925-8388(01)02021-7
13. Agranovski, I.E., Ilyushechkin, A.Y., Altman, I.S., Bostrom, T.E., Choi, M.: Methods of introduction of MgO nanoparticles into Bi-2212/Ag tapes. Phys. C Supercond its Appl. **434**, 115–120 (2006). https://doi.org/10.1016/j.physc.2005.12.005
14. Zhang, S., Li, C., Hao, Q., Feng, J., Lu, T., Zhang, P.: Optimized intergrain connection and Transport properties of Bi-2212 High-Temperature superconductors by Ag nanoparticles inclusions. J. Supercond Nov Magn. **28**, 1729–1736 (2015). https://doi.org/10.1007/s10948-015-2981-1
15. Li, C., Zhang, S., Gao, L., Hao, Q., Bai, L., Zhang, P.: Doping effects of ZrO_2 nanoparticles on the superconducting properties of Bi-2212 tapes. J. Mater. Sci. Mater. Electron. **26**, 3583–3588 (2015). https://doi.org/10.1007/s10854-015-2872-z
16. Jia, Z.Y., Tang, H., Yang, Z.Q., Xing, Y.T., Wang, Y.Z., Qiao, G.W.: Effects of nano-ZrO_2 particles on the superconductivity of Pb-doped BSCCO. Phys. C Supercond its Appl. **337**, 130–132 (2000). https://doi.org/10.1016/S0921-4534(00)00072-1
17. Guo, Y.C., Tanaka, Y., Kuroda, T., Dou, S.X., Yang, Z.Q.: Addition of nanometer SiC in the silver-sheathed Bi2223 superconducting tapes. Phys. C Supercond its Appl. **311**, 65–74 (1999). https://doi.org/10.1016/S0921-4534(98)00625-X
18. Hua, L., Yuan, G., Yoo, J., Kim, H., Chung, H., Qiao, G.: Effect of ultra-fine MgO doping on flux pinning properties of Bi-2223/Ag superconducting tapes. Phys. C Supercond its Appl. 341–348 (2000). https://doi.org/10.1016/S0921-4534(00)01212-0
19. Özkurt, B.: The influence of WO_3 nano-particle addition on the structural and mechanical properties of $Bi_{1.8}Sr_2Ca_{1.1}Cu_{2.1}O_y$ ceramics. J. Mater. Sci. Mater. Electron. **24**, 4233–4239 (2013). https://doi.org/10.1007/s10854-013-1390-0
20. Türk, N., Gündoğmuş, H., Akyol, M., Yakıncı, Z.D., Ekicibil, A., Özçelik, B.: Effect of tungsten (W) substitution on the physical properties of Bi-(2223) superconductors. J. Supercond Nov Magn. **27**, 711–716 (2014). https://doi.org/10.1007/s10948-013-2351-9
21. Verma, P.K., Kaipamangalath, A., Varma, M.R., Bai, V.S.: Non-reactive Nano WO_3 inclusions to Enhance Flux Pinning in Bi-2223 Superconductor composites. IEEE Trans. Appl. Supercond. 1–25 (2023). https://doi.org/10.1109/TASC.2023.3332750
22. Raju, P.M.S., Seshubai, V., Rajasekharan, T.: A generic process to introduce nanoparticles into powder preforms and its application to Infiltration Growth processing of $REBa_2Cu_3O_7$ superconductor. Mater. Chem. Phys. **161**, 59–64 (2015). https://doi.org/10.1016/j.matchemphys.2015.05.004
23. Ravi, S., Bai, S.: Excess conductivity studies in pure and Ag doped 85 K phase in bi-sr-ca-cu-o system. Solid State Commun. **83**, 117–121 (1992). https://doi.org/10.1016/0038-1098(92)90887-F
24. Bai, V.S., Ravi, S., Rajasekharan, T., Gopalan, R.: On the composition of 110 K superconductor in a (Bi,Pb)-Sr-Ca-Cu-O system. J. Appl. Phys. **70**, 4378–4382 (1991). https://doi.org/10.1063/1.349119
25. Ravi, S., Bai, S.: AC susceptibility study in the 85 K phase of the bi-sr-ca-cu-o system. Phys. C Supercond its Appl. **230**, 51–60 (1994). https://doi.org/10.1016/0921-4534(94)90445-6
26. Verma, P.K., Rajasekharan, T., Das, S.C., Surendran, K.P., Bai, S.: Effect of nano ZrO_2 addition on the properties of $Ca_{0.86}Sr_{0.14}CuO_2$ added Bi 2223 composites. J. Phys. Conf. Ser. **2545**, 012014 (2023). https://doi.org/10.1088/1742-6596/2545/1/012014
27. Bai, V.S., Ravi, S., Rajasekharan, T., Gopalan, R.: On the composition of 110 K superconductor in a (Bi,Pb)-Sr-Ca-Cu-O system. J. Appl. Phys. **70**, 4378–4382 (1991). https://doi.org/10.1063/1.349119
28. Chen, D.-X., Hernando, A., Conde, F., Ramírez, J., González-Calbet, J.M., Vallet, M.: Lower critical field and surface barrier in sintered $Bi_2Sr_2CaCu_2O_{8+\delta}$ superconductor. J. Appl. Phys. **75**, 2578–2583 (1994). https://doi.org/10.1063/1.356232
29. Enferadi-Kerenkan, A., Ello, A.S., Do, T.O.: Synthesis, Organo-Functionalization, and Catalytic Properties of Tungsten Oxide nanoparticles as Heterogeneous Catalyst for oxidative cleavage of oleic acid as a model fatty acid into Diacids. Ind. Eng. Chem. Res. **56**, 10639–10647 (2017). https://doi.org/10.1021/acs.iecr.7b03001
30. Shannon, R.D.: Revised effective ionic radii and systematic studies of interatomic distances in halides and chalcogenides. Acta Crystallogr. Sect. A. **32**, 751–767 (1976). https://doi.org/10.1107/S0567739476001551
31. Thoma, M., Shi, Y., Dennis, T., Durrell, J., Cardwell, D.: Effect of Y-211 particle size on the growth of single grain Y-Ba-Cu-O bulk superconductors. J. Cryst. Growth. **412**, 31–39 (2015). https://doi.org/10.1016/j.jcrysgro.2014.11.037
32. Murakami, M.: Processing of bulk YBaCuO. Supercond Sci. Technol. **5**, 185–203 (1992). https://doi.org/10.1088/0953-2048/5/4/001
33. Devendra Kumar, N., Rajasekharan, T., Muraleedharan, K., Banerjee, A., Seshubai, V.: Unprecedented current density to high fields in $YBa_2Cu_3O_{7-\delta}$ superconductor through nano-defects generated by preform optimization in infiltration growth process. Supercond Sci. Technol. **23**, 105020 (2010). https://doi.org/10.1088/0953-2048/23/10/105020
34. Pavan Kumar Naik, S., Devendra Kumar, N., Raju, M.S., Rajasekharan, P., Seshubai, T.: Effect of infiltration temperature on the properties of infiltration growth processed YBCO superconductor. Phys. C Supercond its Appl. **487**, 72–76 (2013). https://doi.org/10.1016/j.physc.2013.01.008
35. Lovleena, Bidikin, I.K., Kholkin, A.L., Kumar, B.: Structural changes in ab-plane of Zn doped Bi-2212 HTSC single crystals. Phys. C Supercond. **451**, 44–48 (2007). https://doi.org/10.1016/j.physc.2006.10.003
36. Goretta, K.C., Todt, V.R., Miller, D.J., Lanagan, M.T., Chen, Y.L., Balachandran, U., Guo, J., Lewis, J.A.: Engineered flux-pinning centres in $Bi_2Sr_2CaCu_2O_x$ and $TlBa_2Ca_2Cu_3O_x$ superconductors. J. Electron. Mater. **24**, 1961–1966 (1995). https://doi.org/10.1007/BF02653017
37. Kazin, P.E., Poltavets, V.V., Poltavets, O.N., Kovalevsky, A.A., Tretyakov, Y.D., Jansen, M.: Formation of Bi-2212 phase and phase assemblage in Ga-doped BSCCO system. Phys. C Supercond its Appl. **324**, 30–38 (1999). https://doi.org/10.1016/S0921-4534(99)00444-X
38. Awana, V.P.S., Agarwal, S.K., Kumaraswamy, B.V., Singh, B.P., Narlikar, A.V.: Effect of 3d metallic dopants on superconductivity

of the Bi $_2CaSr_2Cu_2O_8$ system. Supercond Sci. Technol. **5**, 376–380 (1992). https://doi.org/10.1088/0953-2048/5/6/010
39. Sarun, P.M., Shabna, R., Vinu, S., Biju, A., Syamaprasad, U.: Highly enhanced superconducting properties of Bi-2212 by Y and pb co-doping. **404**, 1602–1606 (2009). https://doi.org/10.1016/j.physb.2009.01.023
40. Gharahcheshmeh, M.H., Galstyan, E., Xu, A., Kukunuru, J., Katta, R., Zhang, Y., Majkic, G., Li, X.-F., Selvamanickam, V.: Superconducting transition width (ΔT_c) characteristics of 25 mol% Zr-added (Gd, Y)$Ba_2Cu_3O_{7-\delta}$ superconductor tapes with high in-field critical current density at 30 K. Supercond Sci. Technol. **30**, 015016 (2017). https://doi.org/10.1088/0953-2048/30/1/015016
41. Gündoğmuş, H., Özçelik, B., Sotelo, A., Madre, M.A.: Effect of Yb-substitution on thermally activated flux creep in the $Bi_2Sr_2CaCu_{2-x}Yb_xO_y$ superconductors. J. Mater. Sci. Mater. Electron. **24**, 2568–2575 (2013). https://doi.org/10.1007/s10854-013-1135-0
42. ÖZTORNACI, U.: The effect of nano-sized metallic au addition on structural and magnetic properties of $Bi_{1.8}Sr_2Au_xCa_{1.1}Cu_{2.1}O_y$ (Bi-2212) ceramics. Ceram. Int. **43**, 4545–4550 (2017). https://doi.org/10.1016/j.ceramint.2016.12.109
43. Bean, C.P.: Magnetization of hard superconductors. Phys. Rev. Lett. **8**, 250–253 (1962). https://doi.org/10.1103/PhysRevLett.8.250
44. Kumar, N.D., Rajasekharan, T., Muraleedharan, K., Banerjee, A., Seshubai, V.: Unprecedented current density to high fields in $YBa_2Cu_3O_{7-\delta}$ superconductor through nano-defects generated by preform optimization in infiltration. (2010). https://doi.org/10.1088/0953-2048/23/10/105020
45. Devendra Kumar, N., Raju, M.S., Pavan Kumar Naik, P., Rajasekharan, S., Seshubai, T.: Effect of preform compaction pressure on the final microstructures and superconducting properties of $YBa_2Cu_3O_{7-\delta}$ superconductors fabricated by directionally solidified Preform optimized infiltration growth process. J. Low Temp. Phys. **174**, 113–127 (2014). https://doi.org/10.1007/s10909-013-0955-x
46. Muralidhar, M., Jirsa, M., Sakai, N., Murakami, M.: Progress in melt-processed (Nd-Sm-Gd)$Ba_2Cu_3O_y$ superconductors. Supercond Sci. Technol. **16** (2003). https://doi.org/10.1088/0953-2048/16/1/201
47. Lacey, D.E., Wilson, J.A.: Low-field flux-creep measurements on YBCO and BSCCO. Supercond Sci. Technol. **5**, 724–731 (1992). https://doi.org/10.1088/0953-2048/5/12/005
48. Salamati, H., Kameli, P.: AC susceptibility study of YBCO thin film and BSCCO bulk superconductors. J. Magn. Magn. Mater. **278**, 237–243 (2004). https://doi.org/10.1016/j.jmmm.2003.12.1311
49. Sharma, D., Kumar, R., Awana, V.P.S.: DC and AC susceptibility study of sol-gel synthesized $Bi_2Sr_2CaCu_2O_{8+\delta}$ superconductor. Ceram. Int. **39**, 1143–1152 (2013). https://doi.org/10.1016/j.ceramint.2012.07.038
50. Zouaoui, M., Ghattas, A., Annabi, M., Ben Azzouz, F., Ben Salem, M.: Effect of nano-size ZrO2 addition on the flux pinning properties of (Bi, Pb)-2223 superconductor. Supercond Sci. Technol. **21** (2008). https://doi.org/10.1088/0953-2048/21/12/125005
51. Koblischka, M.R.: Nanoengineering of flux pinning sites in high-T_c superconductors. Tsinghua Sci. Technol. **8**, 280–291 (2003)
52. Klein, L., Yacoby, E.R., Yeshurun, Y., Erb, A., Müller-Vogt, G., Breit, V., Wühl, H.: Peak effect and scaling of irreversible properties in untwinned Y-Ba-Cu-O crystals. Phys. Rev. B. **49**, 4403–4406 (1994). https://doi.org/10.1103/PhysRevB.49.4403
53. Goto, T., Inagaki, K., Watanabe, K.: Critical current density in filamentary (nd, Sm, Eu, Gd)-Ba-Cu-O superconductors prepared by a solution spinning method. Phys. C Supercond its Appl. **330**, 51–57 (2000). https://doi.org/10.1016/S0921-4534(99)00608-5
54. Murakami, M., Yoo, S.I.: Comparative study of critical current densities and flux pinning among a flux-grown $NdBa_2Cu_3O_y$ single crystal, melt-textured Nd-Ba-Cu-O, and Y-Ba-Cu-O bulks. Phys. Rev. B - Condens. Matter Mater. Phys. **59**, 1514–1527 (1999). https://doi.org/10.1103/PhysRevB.59.1514
55. Vinu, S., Sarun, P.M., Shabna, R., Biju, A., Syamaprasad, U.: Enhancement of flux pinning and Anderson-Dew-Hughes pinning analysis in $Bi_{1.6}Pb_{0.5}Sr_{2-x}$ $Tb_xCa_{1.1}Cu_{2.1}O_{8+\delta}$ superconductor. J. Alloys Compd. **477**, 13–16 (2009). https://doi.org/10.1016/j.jallcom.2008.10.033
56. Kramer, E.J.: Scaling laws for flux pinning in hard superconductors. J. Appl. Phys. **44**, 1360–1370 (1973). https://doi.org/10.1063/1.1662353
57. Rose, R.A., Ota, S.B., de Groot, P.A.J., Jayaram, B.: Scaling of the vortex pinning force in $Bi_2Sr_2CaCu_2O_{8+y}$. Phys. C Supercond its Appl. **170**, 51–55 (1990). https://doi.org/10.1016/0921-4534(90)90227-6
58. Leveratto, A., Armenio, A.A., Traverso, A., De Marzi, G., Celentano, G., Malagoli, A.: Transport current and magnetization of Bi-2212 wires above liquid helium temperature for cryogen-free applications. Sci. Rep. **11**, 1–9 (2021). https://doi.org/10.1038/s41598-021-91222-2
59. Koshelev, A.E., Sadovskyy, I.A., Phillips, C.L., Glatz, A.: Optimization of vortex pinning by nanoparticles using simulations of the time-dependent Ginzburg-Landau model. Phys. Rev. B. **93**, 1–5 (2016). https://doi.org/10.1103/PhysRevB.93.060508
60. Civale, L.: Vortex pinning and creep in high-temperature superconductors with columnar defects. Supercond Sci. Technol. **10** (1997). https://doi.org/10.1088/0953-2048/10/7A/003
61. Zhang, S., Liang, M., Li, C., Hao, Q., Feng, J., Zhang, P.: Enhanced flux pinning properties in Bi-2212 high temperature superconductors with nano-sized precipitates. Mater. Lett. **157**, 197–200 (2015). https://doi.org/10.1016/j.matlet.2015.05.096
62. Qiu, L.P., Zhang, Y.R., Gao, S.L., Zheng, Q.H., Zhang, T.T., Cheng, G.T., Cao, S., ze, Hang, W.P., Ramakrishna, S., Long, Y.Z.: Fabrication and magnetic properties of SiO_2 nanoparticles-doped BSCCO superconducting nanofibers by solution blow spinning. Phys. C Supercond its Appl. **608**, 1354251 (2023). https://doi.org/10.1016/j.physc.2023.1354251